

Natural characteristic analysis of wind turbine drivetrain considering flexible supporting

Proc IMechE Part C:
J Mechanical Engineering Science
0(0) 1–15
© IMechE 2017
Reprints and permissions:
sagepub.co.uk/journalsPermissions.nav
DOI: 10.1177/0954406217692006
journals.sagepub.com/home/pic



Zhang Shenglin, Zhu Caichao, Song Chaosheng,
Tan Jianjun and Chen Xu

Abstract

The mechanical system of wind turbine is much complicated and can be divided into the drivetrain and supporting portions. The drivetrain consists of wheel, main shaft, gearbox, generator, etc. and the supporting portion mainly consists of a tower and a cabin. In order to reduce the unit cost of electricity, the capacity and size of wind turbine are increased gradually in the past years. Meanwhile, with the increase of the wind turbine height, the tower actually becomes more flexible as the supporting part. And the influence of the supporting tower flexibility becomes stronger due to the varying wind loads both in magnitude and direction. Using the rigid–flexible coupling multibody dynamic theory, the coupled dynamic model of the wind turbine drive train was developed considering the flexible supporting. Then the natural characteristics of the system were computed and investigated. For the dynamic modeling, the blades, the tower and main shaft were modeled as flexible bodies, while the other components, such as the hub and the gearbox, were modeled as rigid bodies. The potential resonance frequencies of the system were discussed through the Campbell diagram and the modal energy distribution analysis. The results show that the natural frequency of swing mode shapes for the tower was 0.399 Hz and 0.405 Hz. The first natural frequency of drivetrain, which represented a torsional vibration mode, was 1.64 Hz. From the Campbell diagram and the modal energy distribution analysis, resonances would not occur within the normal operating speed range for the drivetrain. And a comparison analysis indicated that the flexible supports would increase the bearing loads along axial direction and radial direction, especially in main shaft and torque arm, but that influence was not obvious at parallel stage. However, to some extent, the flexible supports can decrease the loads fluctuation of drivetrain. Finally, the online vibration experiments were carried out in the wind field. The vibration characteristics of the wind turbine drivetrain were analyzed and the experimental results also compared well with the theoretical dynamic results.

Keywords

Wind turbine drivetrain, flexible supporting, natural characteristics, experimental study

Date received: 1 August 2016; accepted: 12 January 2017

Introduction

With the development of the wind power technology, the capacity and size of wind turbine grow gradually^{1,2} to reduce the unit cost of electricity. And the tower actually becomes more flexible due to the increase of the tower height.^{3,4} Also, since wind turbines are always installed on mountains, deserts and beaches, the wind loads show an obvious time-varying characteristic due to the change for the sunlight, the topography and the temperature.⁵ Thus, the ranges of the operating speed and excitation frequencies of the system are quite broad. The system may encounter resonances which would cause quite significant vibration and affect the normal operating of the wind

turbine. Also, the time-varying wind loads actually induce the towers to swing seriously due to the coupling effects of the drivetrains inertial force and the aerodynamic load. Therefore, the working performance and life of the wind turbine drivetrain will be influenced directly and it may lead to the failure of drivetrain.

The State Key Laboratory of Mechanical Transmissions, Chongqing University, Chongqing, China

Corresponding author:

Zhu Caichao, Chongqing University, No. 174, Shazhengjie, Shapingba, Chongqing 400044, China.
Email: cczhu@cqu.edu.cn

In recent years, there are a number of studies on the wind turbine drivetrain. Stol and Bir⁶ Stol et al.⁷ built a computational structure dynamic model for a horizontal axis wind turbine. The dynamic response of the model was studied and compared to a model built in ADAMS, etc. Todorov et al.⁸ built a model of wind turbine drivetrain which consists of 10 bodies and investigated the natural frequencies, mode shapes and time series of torsional oscillations. Ahlström⁹ developed a finite model to investigate the non-linear influence of aerodynamics characteristic and tower-shadow effect on horizontal axis wind turbine. Girsang et al.¹⁰ studied a new model of wind turbine drivetrain built in MATLAB/Simulink. Taking the detail generator model into consideration, they analyzed the effects of internal excitation and external excitation for drivetrain. Peeters et al. presented three types of multibody dynamic wind turbine models including the torsional model, the rigid multibody model and the flexible multibody model.^{11–13} Lee et al.¹⁴ performed the structure dynamic analysis of horizontal wind turbine with both rigid- and flexible-body subsystems and analyzed the natural characteristics of this rigid–flexible coupling model.¹⁵ The wind turbine drivetrain is operated with varying loads excitation. As a consequence, it can cause the gearbox to be more prone to failure. Hence, Oyague¹⁶ deeply researched the failure mechanism of gear pairs and bearings in gearbox based on the multibody dynamic software FSAT. And the related research showed that the main shaft bearing in the horizontal axis wind turbine of three-point suspension had a higher risk of failure,¹⁷ so it is necessary to investigate the dynamics of wind turbine drivetrain of three-point suspension. Zhu et al.^{18–20} built the dynamic model of wind turbine drivetrain with rigid–flexible coupling method, analyzed the natural characteristics of that drivetrain model, and compared the simulation results with the experimental results. Muyeen et al. used two-mass, three-mass and six-mass drivetrain models to analyse the transient behavior of wind turbine drivetrain.^{21,22} In recent years, the multibody dynamics simulation software SIMPACK can have a good approximation between simulated and experimental results, which can guide the structural design of wind turbine in reality.^{23,24} Xing²⁵ investigated the comparisons of the different mounting structures for spar-type floating wind turbine and onshore wind turbine to reveal that nacelle motions have relatively significant contributions to the axial bearing forces of planetary stage. However, the wind turbine drivetrain is a strongly coupled structure system with flexible tower, the dynamic response of wind turbine drivetrain considering the flexible supports of tower needs to be further studied.

In this paper, the dynamic theory for the rigid–flexible coupled system was applied to develop a dynamic wind turbine drivetrain model with flexible supporting. The natural characteristics and dynamic

responses of the system were studied theoretically and experimentally. The results can provide guidance for the design optimization of the wind turbine drivetrain.

Structural composition and transmission principle of the wind turbine drivetrain

A typical horizontal axis wind turbine is shown in Figure 1(a).²⁶ Usually, it can be divided into the drivetrain and supporting portion according to their functionality. Drivetrain, which consists of blades, hub, main shaft, gearbox, etc., is the most important and complex component of the wind turbine mechanical system.²⁰ The blades are fixed on the hub by pitch bearings and the hub is fixed on the top of the main shaft by flange. The main shaft is connected to the carrier of the gearbox by locking plate and the high-speed shaft of the gearbox is connected to the generator through coupler. The supporting portion consists of tower and cabin. The cabin is fixed on the top of the tower by yaw bearing, while the tower is fixed on the ground by flange plate. The drivetrain is fixed on the supporting portion through three points, main shaft bearing point and two torque arms

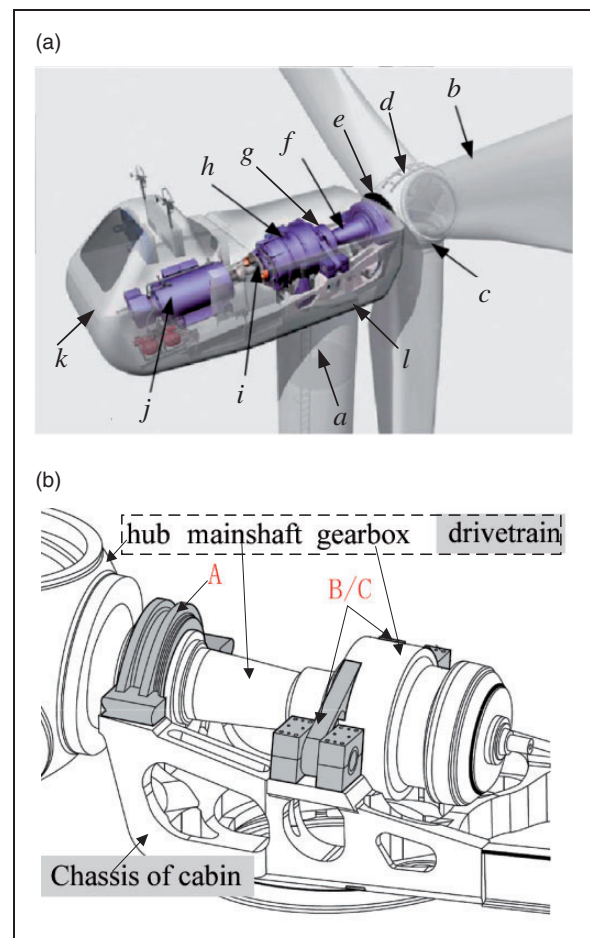


Figure 1. The structure diagram of wind turbine. (a) The components of wind turbine and (b) The connecting points between the drivetrain and the supporting portion.

points of the gearbox as shown in Figure 1(b).²⁷ The symbols appearing in Figure 1 are shown in Table 1.

Based on the assembly relations and transmission principle, the topological diagram of wind turbine drivetrain and supporting portion was built to show

Table 1. Symbols in the structure diagram of wind turbine.

Symbol	Meaning	Symbol	Meaning
<i>a</i>	Tower	<i>g</i>	Locking plate
<i>b</i>	Blade	<i>h</i>	Gearbox
<i>c</i>	Pitch bearing	<i>i</i>	Coupling
<i>d</i>	Hub	<i>j</i>	Generator
<i>e</i>	Flange	<i>k</i>	Cabin
<i>f</i>	Main shaft	<i>l</i>	Yaw bearing

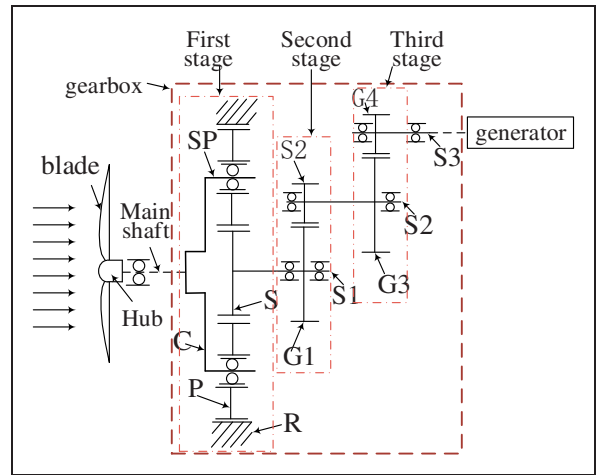


Figure 3. The transmission principle of wind turbine drivetrain.

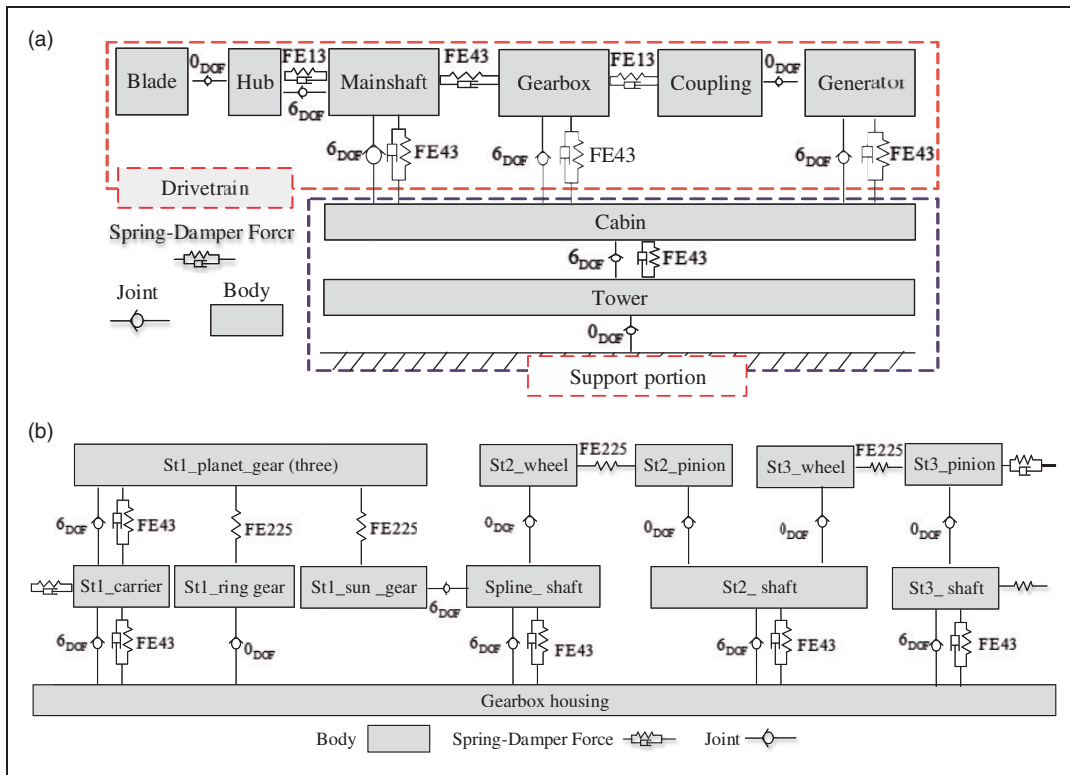


Figure 2. The topological diagram: (a) wind turbine drivetrain and (b) gearbox.

Table 2. Main parameters of the wind turbine.

Power	Ratio	Designed life	Blade length	Blade number	Mass of wind wheel	Cut-in wind speed
2 MW	115.2	20 Years	39 m	3	38t	3 m/s
Rated wind speed	Cut-out wind speed	Button diameter of tower	Top diameter of tower	Height of tower	Type	Rated speed
10 m/s	26 m/s	4.2 m	3.05 m	80.6 m	Double-fed	1790 r/min

the connections, the relative freedoms and the interaction forces between components. The total topological diagram is shown in Figure 2(a) and the detail topological diagram of gearbox is shown in Figure 2(b). In this diagram, the components are represented by “bodies” and the relative freedoms of components are represented by “joints,” while the forces are represented by “spring-damper.”

In this work, a common 2 MW horizontal axis wind turbine was taken as an example to investigate the natural characteristics of the wind turbine drivetrain. The main parameters of the wind turbine are shown in Table 2. The structure and transmission principle of the drivetrain are shown in Figure 3. The blades are the input and the generator is the output. The corresponding symbols are explained in Table 3.

Wind turbine gearbox is the most complex part of the drivetrain and the common structure of gearbox is shown in Figure 3. The carrier is the input of the gearbox and the high-speed shaft is the output. The first stage is planetary gear transmission with three planets circumferentially equispaced on the carrier. The second and third stages are parallel transmission and the wheel of the second stage is connected to the sun gear of the first stage. The pinion of the third stage is connected to the generator through coupler. The main parameters for the gearbox transmission system are listed in Table 4.

Dynamic modeling and natural characteristics analysis

Dynamic model for the drivetrain considering flexible supporting

The dynamic model is simplified according to the topological diagram. For the dynamic modeling,

Table 3. Symbols in the transmission principle of wind turbine drivetrain.

Symbols	C	P	R	S	G_i	S_i
Meaning	Planet carrier	Planet gear	Ring gear	Sun gear	Outer gear i	Shaft i

the blades, main shaft and tower were modeled as flexible bodies, and other components are modeled as rigid bodies. For example, the simplified model of main shaft is shown in Figure 4. And a flexible main shaft was used in the model and three master points, “main shaft_hub” marker, “main shaft_cabin” marker and “main shaft_carrier” marker were used to connect to other corresponding components. Other linking positions of the rigid bodies are simplified similarly to the main shaft. And the first six modal freedoms of every blade and the first 10 modal freedoms of tower are considered according to Guideline for the Certification of Wind Turbines.²⁸

The bodies were assembled by joints and the relative freedoms of the bodies were set according to the assembly relationship. The joints in the wind turbine drivetrain are listed in Figure 5(a) and Table 5. The body j is fixed on the body i which had six degree of freedoms. The mass and moment of inertia for generator were considered as shown in Figure 5(c). Based on the mounting structure, the generator was supported by up-wind and down-wind bearings mounted on the cabin, which was simulated by FE

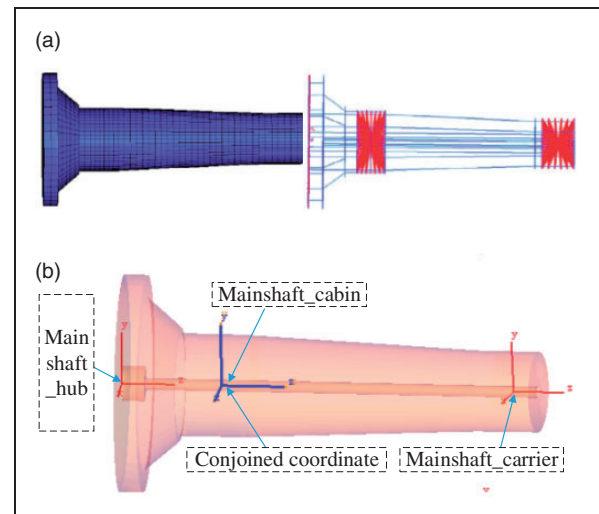


Figure 4. The simplified structure of the main shaft. (a) FE reduction model of the main shaft and (b) the assembly connection of main shaft.

Table 4. Main parameters of the wind turbine gearbox.

Parameters		Number of teeth	Modulus/mm	Helical angle/ $^{\circ}$	pressure angle/ $^{\circ}$	Ratio	Tooth Width/mm
The first stage	Sun	21	15	8	25		395
	Planet	37	15	8	25	5.5	390
	Ring	96	15	8	25		395
The second stage	The gear	97	11	10	20		310
	The wheel	23	11	10	20	4.2	320
The third stage	The gear	103	8	10	20		180
	The wheel	21	8	10	20	4.9	190

43 in SIMPACK. The value of bearing stiffness was acquired by KiSSsoft. As an element to connect high-speed shaft with generator, the structure of coupling was complex, and hence it could be simplified to spring dampers simulated by the FE 13 in SIMPACK. The stiffness property of the coupling was 7.5×10^6 Nm/rad. And the damping of coupling could be calculated by following equation

$$d = 2D\sqrt{KI} \quad (1)$$

where K is the torsional stiffness, I is the moment of inertia and damping factor D is set to 0.4.

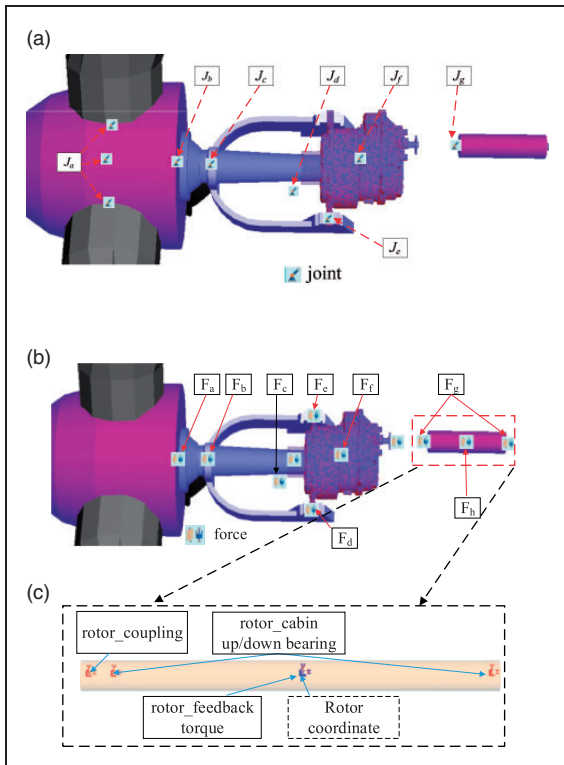


Figure 5. The joints and forces relationship diagram of the wind turbine drivetrain.

Table 5. Relative degrees of freedom of the wind turbine drivetrain and supporting portion.

Joint	Body j	Body i	Freedom	Freedoms
J_b	Hub	Main shaft	6 _{DOF}	$x/y/z/\alpha/\beta/\gamma$
J_c	Main shaft	Cabin	6 _{DOF}	$x/y/z/\alpha/\beta/\gamma$
J_e	Gearbox	Cabin	6 _{DOF}	$x/y/z/\alpha/\beta/\gamma$
J_f	Carrier etc.	Gearbox	48 _{DOF}	$x/y/z/\alpha/\beta/\gamma$
J_g	Generator	Cabin	6 _{DOF}	$x/y/z/\alpha/\beta/\gamma$
J_d	Cabin	Tower	6 _{DOF}	$x/y/z/\alpha/\beta/\gamma$
J_a	Blade	Hub	0 _{DOF}	The first six modal freedoms
J_h	Tower	Ground	0 _{DOF}	The first 10 modal freedoms

Force elements were created between bodies according to the transmission principle and the assembly relationship of drivetrain as shown in Figure 5(b) and Table 6.

For the bearings in the model, including the main shaft bearing and other bearings in the gearbox, the bearing stiffness was represented as a spring damper FE43 in SIMPACK. For the force elements of bearing, diagonal 6×6 stiffness and damping matrices were used and the connecting relation between body 1 and body 2 can be shown as in the following

$$\begin{bmatrix} F_{body,1} \\ F_{body,2} \end{bmatrix} = K_{Bearing} \begin{bmatrix} q_{body,1} \\ q_{body,2} \end{bmatrix} + C_{Bearing} \begin{bmatrix} \dot{q}_{body,1} \\ \dot{q}_{body,2} \end{bmatrix} \quad (2)$$

with

$$K_{Bearing} = \begin{bmatrix} k_{x,x} & 0 & 0 & 0 & 0 & 0 \\ 0 & k_{y,y} & 0 & 0 & 0 & 0 \\ 0 & 0 & k_{z,z} & 0 & 0 & 0 \\ 0 & 0 & 0 & k_{\theta,x} & 0 & 0 \\ 0 & 0 & 0 & 0 & k_{\theta,y} & 0 \\ 0 & 0 & 0 & 0 & 0 & 0 \end{bmatrix},$$

Table 6. Symbols in the force relationship of the system.

Force	Body j	Body i	Force	Body j	Body i
F_a	Hub	Main shaft	F_e	Torque arm of gearbox	Cabin
F_b	Main shaft	Cabin	F_g	Generator	Cabin
F_c	Cabin	Tower	F_h	Generator	Cabin
F_d	Torque arm of gearbox	Cabin	F_f	Components of gearbox	Gearbox

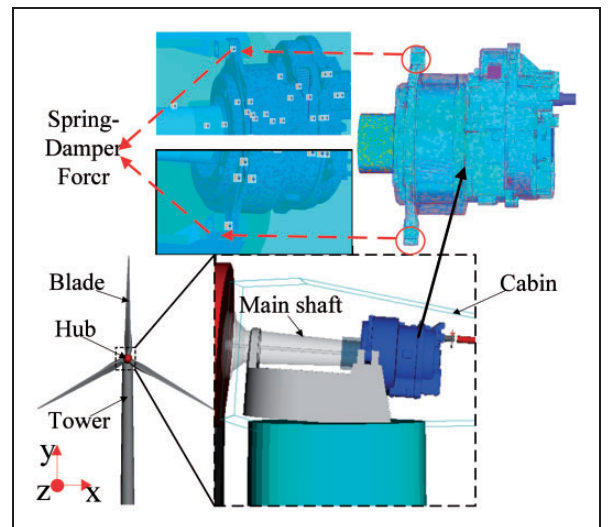


Figure 6. The final model of wind turbine drivetrain with flexible supporting.

$$C_{\text{Bearing}} = \begin{bmatrix} c_{x,x} & 0 & 0 & 0 & 0 & 0 \\ 0 & c_{y,y} & 0 & 0 & 0 & 0 \\ 0 & 0 & c_{z,z} & 0 & 0 & 0 \\ 0 & 0 & 0 & c_{\theta x} & 0 & 0 \\ 0 & 0 & 0 & 0 & c_{\theta y} & 0 \\ 0 & 0 & 0 & 0 & 0 & 0 \end{bmatrix} \quad (3)$$

Table 7. The first 25 order natural frequencies of the drive train.

Order	Frequencies/ Hz	Order	Frequencies/ Hz	Order	Frequencies/ Hz
1	1.64	10	45.5	19	648.8
2	2.08	11	60.8	20	737.3
3	3.4	12	79.1	21	1058.2
4	5.7	13	113.6	22	1081.4
5	8.2	14	149.6	23	1167.2
6	9.74	15	242.1	24	1357.4
7	20.1	16	294.05	25	1968.1
8	22.8	17	359.15		
9	34.9	18	507.9		

where $F_{\text{body},i}$ ($i=1,2$) is the acting force between body 1 and body 2, K_{Bearing} (C_{Bearing}) is the stiffness (damping) matrix of the bearing element. And $q_{\text{body},i}$ ($i=1,2$) is the generalized degrees of freedom for body i . And $k_{i,i}$ ($c_{i,i}$) ($i=x, y, z, \theta x, \theta y$) is the corresponding stiffness (damping) of each freedom.

The dynamic drivetrain model considering flexible supporting is shown in Figure 6 with total 100 degrees of freedom. Finally, the commercial software SIMPACK was used to solve the dynamic model.

Natural characteristics analysis of the drivetrain

The dynamic differential equation of the system can be expressed as

$$[M]\{\ddot{z}\} + [C]\{\dot{z}\} + [D]\{z\} = \{F\} \quad (4)$$

where $[M]$, $[C]$ and $[D]$ are the mass, stiffness and damping matrix of the system, respectively. $\{\ddot{z}\}$, $\{\dot{z}\}$ and $\{z\}$ are the vectors of the accelerations, speeds and displacements, respectively. $\{F\}$ is the load vector.

By solving the proposed dynamic model, the first 25 order natural frequencies of the system are listed in Table 8. The 1st order is the “fundamental

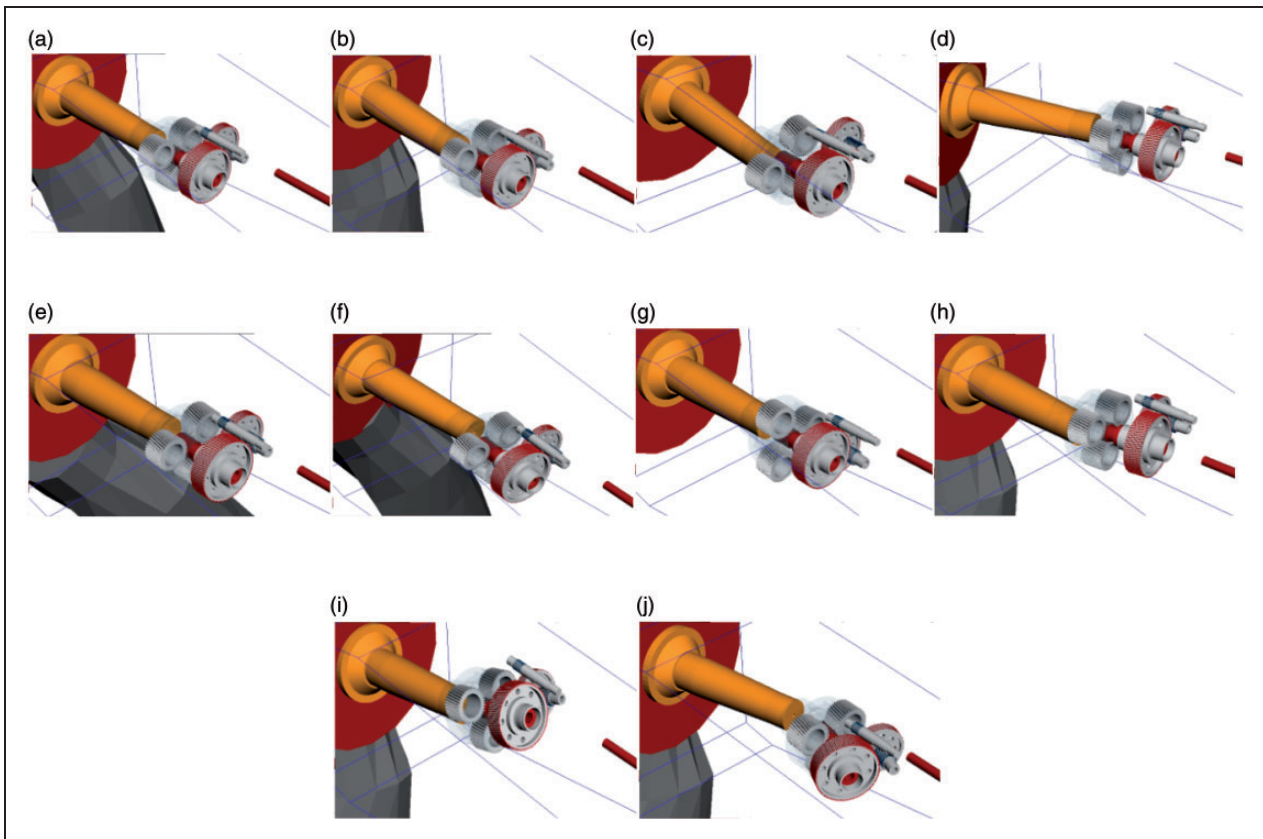


Figure 7. Vibration modes of the wind turbine drive train. (a) mode 1, (b) mode 2, (c) mode 3, (d) mode 4, (e) mode 5, (f) mode 6, (g) mode 7, (h) mode 8 (i) mode 9 and (j) mode 10.

frequency” of the drivetrain. The first 10 order mode shapes are shown in Figure 7. Additionally, it should be noted that the natural frequencies 0.399 Hz and 0.405 Hz represent the natural frequency of swing mode shapes for the tower in the z- and x-directions, respectively.

In order to verify the simulation results, the “fundamental frequency” of the drivetrain verification is performed according to GL2010.²⁸ The “fundamental frequency” of the drivetrain calculation can be calculated by

$$f = \frac{\sqrt{k/I}}{2\pi} \quad (5)$$

where k is the torsional stiffness of the drivetrain and I is the moment of inertia. The torsional stiffness can be represented by

$$k = [(3k_b)^{-1} + k_d^{-1}]^{-1} \quad (6)$$

where k_b is the torsional stiffness of the blade with the value 1.64×10^8 Nm/rad calculated by the equation $k_b = 4I\pi^2 f^2$, where I is the moment of inertia and f is the natural frequency of shimmy mode for blade. k_d is the equal torsional stiffness of the drivetrain excluding the blades. The generator stator and generator rotor were fixed in dynamics model, then the torque $T_1=500$ KNm and $T_2=1000$ KNm are applied to the torsional freedom of hub, sequentially. After the drive train became static equilibrium, the rotational angle hub are recorded as α_1 and α_2 as shown in Figure 8. Then the torsional stiffness can be calculated by

$$k_d = \frac{T_2 - T_1}{\alpha_2 - \alpha_1} = 1.59 \times 10^8 \text{ Nm/rad} \quad (7)$$

The moments of inertia of hub, main shaft, and the shafts in the gearbox were ignored compared to the moments of inertia of blades and generator.

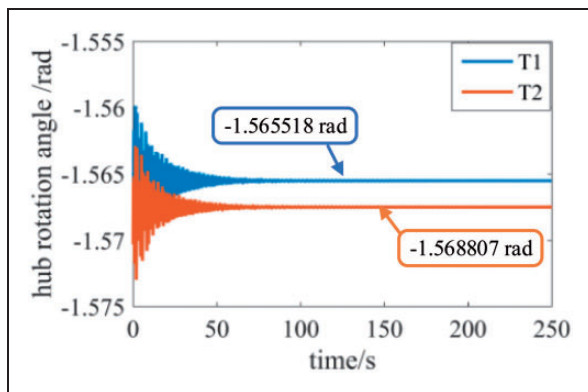


Figure 8. The rotation angles of hub with T_1 (500 KNm) and T_2 (1000 KNm).

The calculation of I can be applied using the following formula.

$$I = \frac{3I_b I_g u^2}{I_g u^2 + 3I_b} = 1.02 \times 10^6 \text{ kgm}^2 \quad (8)$$

where I_g is moments of inertia of generator, u is the transmission ratio of the drivetrain, I_b is moments of inertia of blade.

Finally, the theoretical “fundamental frequency” of the drivetrain is 1.72 Hz according to equation (5). The deviation is $|1.64-1.72|/1.64 \times 100\% = 4.8\% < 5\%$, which compares well with GL demand.

The potential resonance analysis

The theoretical shaft frequencies and mesh frequencies of gear pairs-under cut-in, rate and cut-out speed are shown in Table 8. Since the rotational speed of blades, hub and main shaft is the same, only the rotational speed of the main shaft is shown. The main frequencies considered are the first order, second order, third order and sixth order of the main shaft

Table 8. Excitation frequencies of drive train.

Rotate speed (r/min)	Cut-in speed Rate speed Cut-out speed		
	1050	1790	1900
Shaft frequency (Hz)			
Rotor_1p	0.1518	0.2589	0.2748
Rotor_2p	0.3037	0.5177	0.5495
Rotor_3p	0.4555	0.7766	0.8243
Rotor_6p	0.9111	1.5532	1.6486
shaft 1_1p	0.846	1.4422	1.5309
shaft 1_2p	1.692	2.8845	3.0618
shaft 2_1p	3.568	6.0825	6.4563
shaft 2_2p	7.1359	12.165	12.9126
shaft 3_1p	17.5	29.8333	31.6667
shaft 3_2p	35	59.6667	63.3333
Gear mesh frequency (Hz)			
mesh1_1p	14.5774	24.851	26.3782
mesh1_2p	29.1549	49.7021	52.7564
mesh1_3p	43.7322	74.553	79.1346
mesh2_1p	82.0631	139.8981	148.4951
mesh2_2p	164.1262	279.7961	296.9903
mesh2_3p	246.1893	419.6943	445.4853
mesh3_1p	367.5	626.5	665
mesh3_2p	735	1253	1330
mesh3_3p	1102.5	1879.5	1995

Rotor_ip: main shaft frequency; shaft 1_ip: shaft frequency of low-speed shaft; shaft 2_ip: shaft frequency of intermediate-speed shaft; shaft 3_ip: shaft frequency of high-speed shaft, mesh1_ip: mesh frequency of planetary stage, mesh2_ip: mesh frequency of intermediate speed gear stage; mesh3_ip: mesh frequency of high speed gear stage, where i means the i th order and p means harmonic.

frequency, the first and second order of the low-speed shaft frequency, intermediate-speed shaft frequency and high-speed shaft frequency, first order, second order and third order of the mesh frequencies for each gear pair.²⁸

Figure 9 shows the Campbell diagram according to the results in Table 8. The intersection points of natural frequencies and excitation frequencies mean the potential resonances. The risk frequencies and the excitation frequencies are listed in Table 9.

The vibration strength of the components in the system has a strong relation with the modal energy distribution. Higher modal energy means stronger vibration for the component under specified excitation. The modal energy calculation method of component $T_i^{(n)}$, the modal energy of the system of the n th order $T^{(n)}$ and the percentage of the modal energy of the i th component accounted for the system $P_i^{(n)}$ are shown as follows

$$\begin{cases} T_i^{(n)} = \frac{1}{2} \omega_n^2 (\Phi_n^T)_i M_i (\Phi_n)_i \\ T^{(n)} = \sum \frac{1}{2} \omega_n^2 (\Phi_n^T)_i M_i (\Phi_n)_i \\ P_i^{(n)} = \frac{T_i^{(n)}}{T^{(n)}} \times 100\% \end{cases} \quad (9)$$

where ω_n, Φ_n are the n th order natural frequency and the vector of the n th order mode shape of the system, respectively. $(\Phi_n)_i$ is the vector of the i th component

of the n th order mode shape, M is the matrix of the mass, M_i is the matrix of the mass of i th component.

Figure 10 shows the modal energy distributions of the first four orders listed in Table 7. It can be seen that the modal energy for the first and second order is mainly concentrated in the blades and generator. The modal energy for the third order and fourth order is mainly located at the blades.

The results of the Campbell diagram shown in Figure 9(c) indicate that the first order natural

Table 9. Risk frequencies and corresponding excitation frequencies.

Natural frequency (order)	Excitation frequency	Natural frequency (order)	Excitation frequency
1st	Rotor_6p	10th	mesh1_3p
1st,2nd	shaft1_2p	14th	mesh2_1p
4th	shaft2_1p	15th,16th	mesh2_2p
5th,6th	shaft2_2p	16th,17th	mesh2_3p
7th	shaft3_1p	18th,19th	mesh3_1p
9th,10th,11th	shaft3_2p	20th,21th,22th,23th	mesh3_2p
7th	mesh1_1p	23th,24th,25th	mesh3_3p
9th,10th	mesh1_2p		

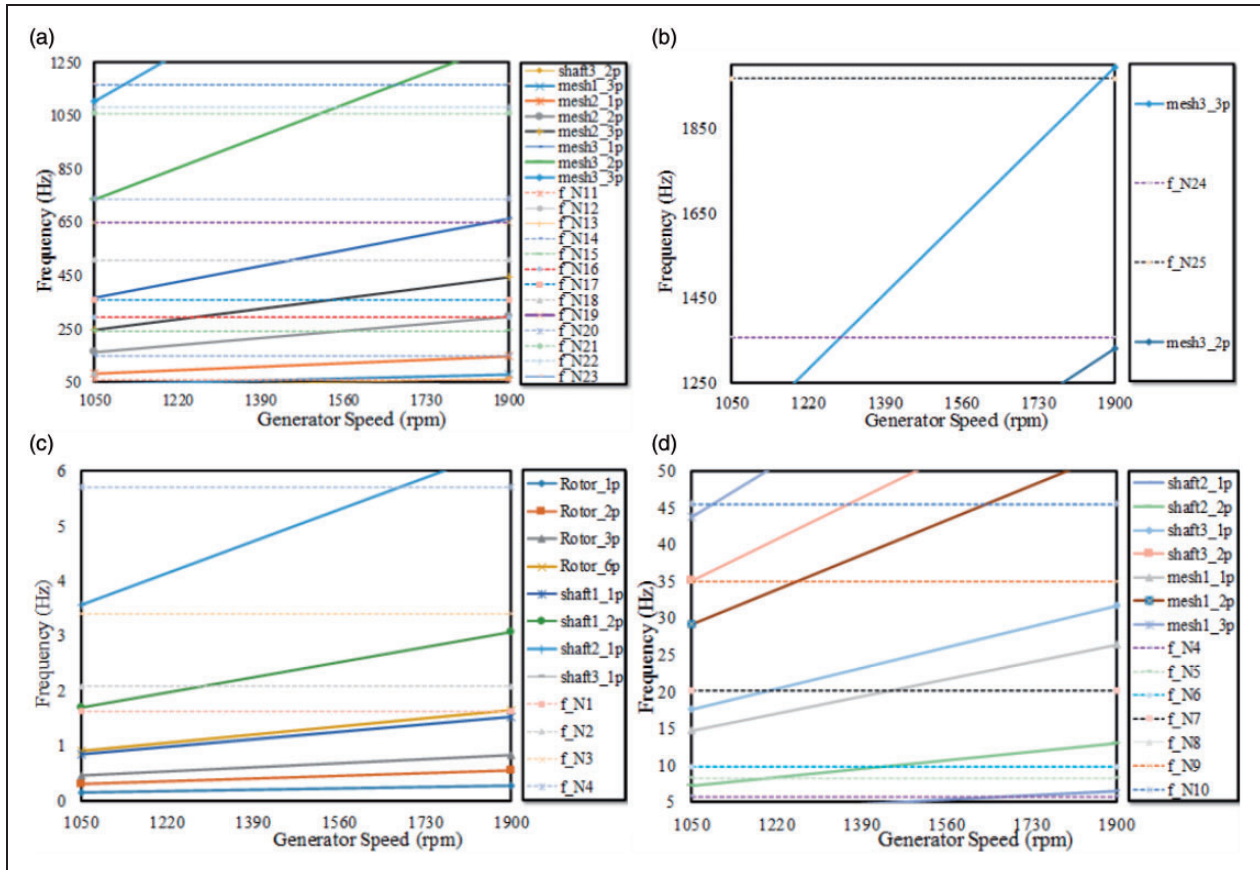


Figure 9. Campbell diagram of wind turbine drivetrain. (a) 50–1250 Hz (b) 1250–2000 Hz (c) 0–5 Hz and (d) 5–50 Hz.

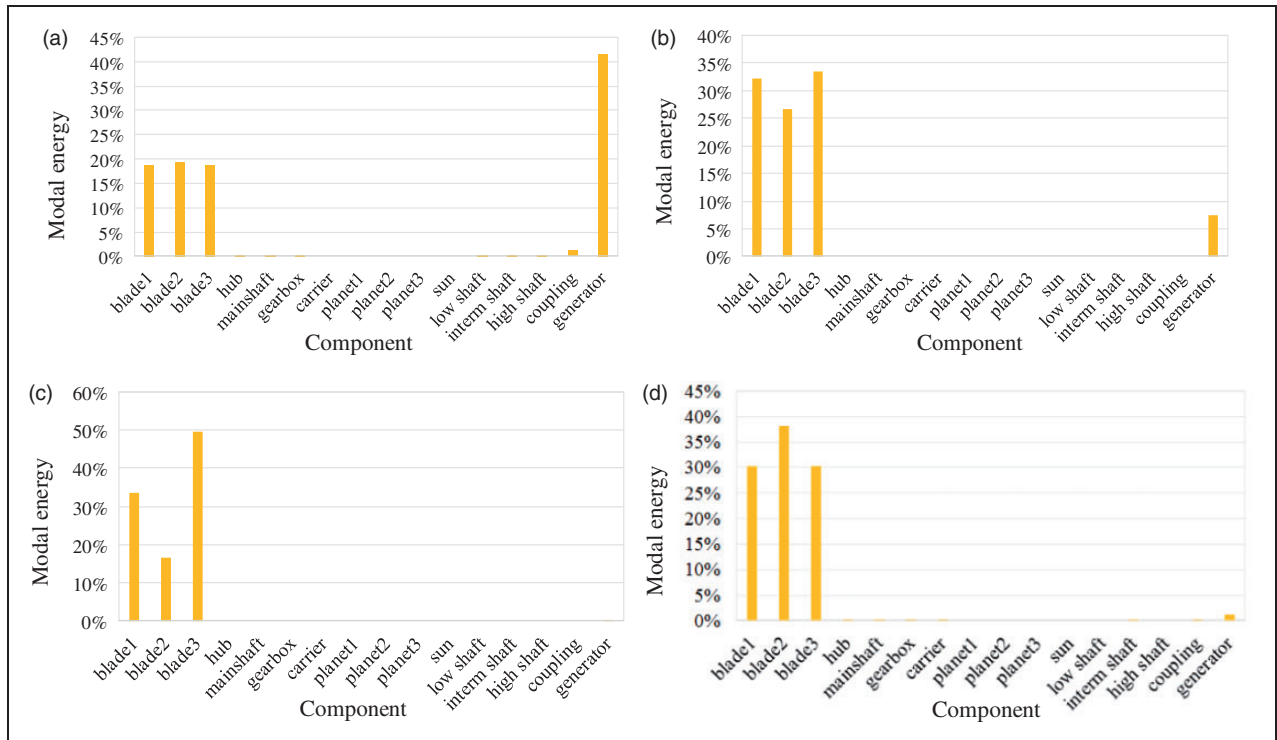


Figure 10. Modal energy distribution histogram of components in the wind turbine. (a) Mode 1, (b) Mode 2 (c) Mode 3 and (d) Mode 4.

frequency intersects with the sixth harmonic of the main shaft frequency. However, the main modal energy does not coincide with the frequency intersection according to Figure 10(a). Thus, resonance will not happen with the first order of natural frequency. Also, further studies indicate that resonance will not happen with the other order natural frequencies.

Comparisons of internal drivetrain responses

The comparisons of the bearing forces for main components, including main shaft, torque arm, carrier, planet and shaft₃, with different wind speed are presented in Figures 11 to 13. The related results are shown by the percentage difference of the response considering flexible supports (FS) versus the response with rigid supports (RS)

$$\% \text{ difference} = \frac{X_{RS} - X_{FS}}{X_{FS}} \times 100\% \quad (10)$$

where X_{RS} is the dynamic bearing force and mesh force of drivetrain considering rigid supports, similarly, X_{FS} is the dynamic bearing force and mesh force of drivetrain considering flexible supports.

As we know, the theoretical value of pitch angle is 0° , while the wind speed is lesser than the rated wind speed. For our calculation, the wind speed from 3 m/s to 10 m/s is taken into consideration; hence, the pitch control system can be ignored in the wind turbine drive train reasonably. Besides, the feedback torque

of generator is determined by torque–speed curve measured at experimental measurement.

From the results, with increase of wind load, there is a gradually decreasing tendency of mean values and maximum values in main shaft, planetary stage and high-speed stage for the rigid support condition compared with the flexible support condition. Intuitively, the wind load is directly transferred by main shaft and applied to the components along the axial direction, while the axial stiffness is lesser than radial stiffness; hence, the axial load distribution can be affected by flexible supports more obviously. On the other hand, the rigid supports can increase the standard deviation, especially in lower wind load level compared with flexible supports.

From Figure 12, it is seen that the flexible support can increase the mean loads of main shaft and torque arm, which coincides with the trend of the mean values of planetary stage presented in Figure 11. However, that flexible support decreases the mean loads of planetary stage. And there is an increasing tendency of maximum bearing loads at main shaft, torque arm, carrier and high-speed stage. Inversely, that maximum values can be decreased at planet bearing compared with the flexible support. Besides, the flexible support can significantly reduce the standard deviation of radial bearing force, especially in high-speed stage.

As seen in Figure 13, there is a more increase in the mean tooth contact force at planetary stage than that at parallel stage compared with flexible supports.

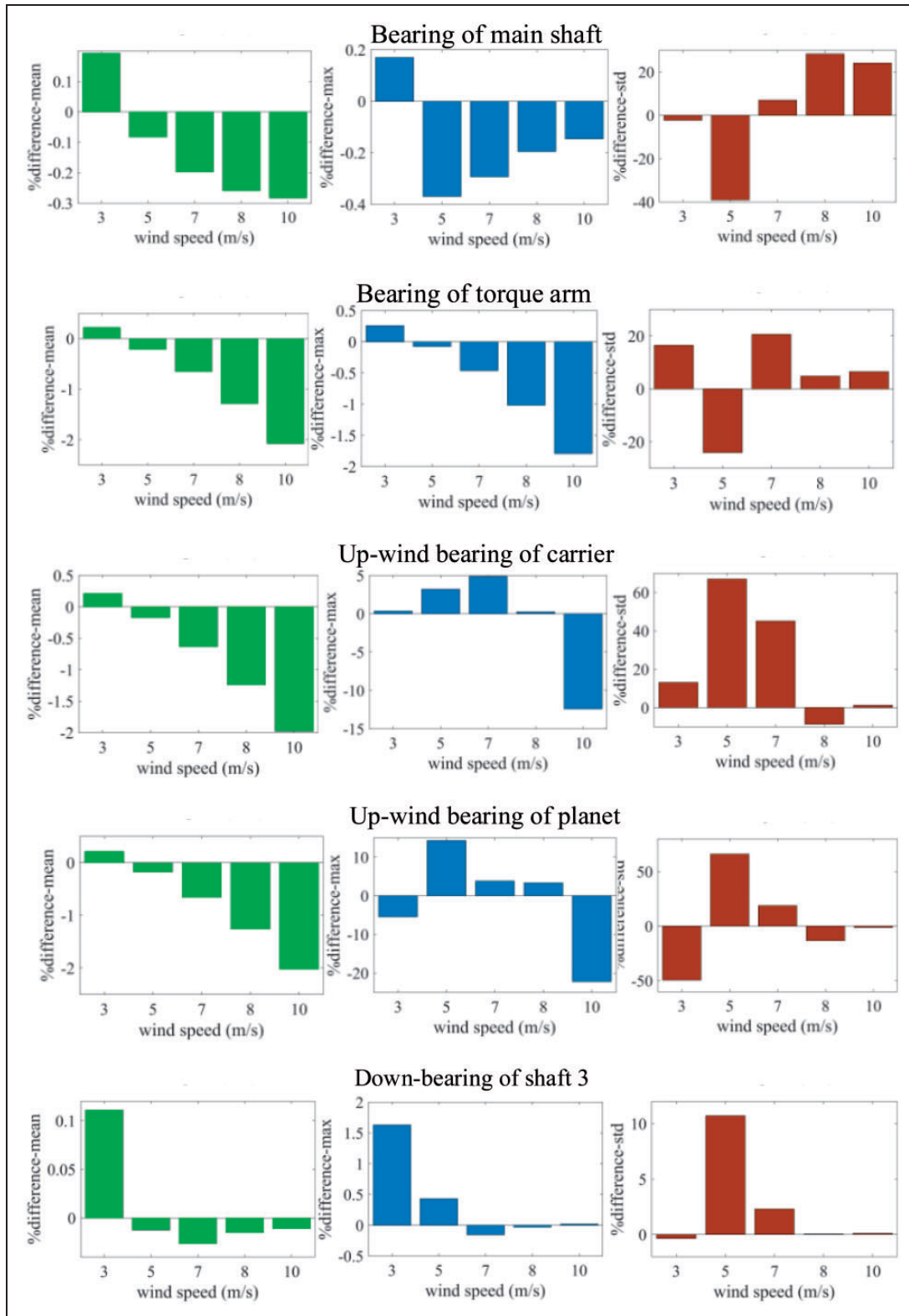


Figure 11. Comparisons of mean values, maximum values and standard deviations along the z-direction. (a) Bearing of main shaft, (b) bearing of torque arm, (c) upwind bearing of carrier, (d) upwind bearing of planet and (e) downbearing of shaft 3.

And the similar trends can be seen at maximum bearing forces. It can be explained that flexible supports can act as a role to isolate the fluctuation of external loads. And there are also increases in the standard deviations of the tooth contact forces compared with flexible supports, especially in lower wind load level.

Wind field test of the wind turbine drive train

In order to verify the simulation results, a remote real-time measurement system for wind turbine drive train was developed using SKF Windcon.²⁹ Dynamic data

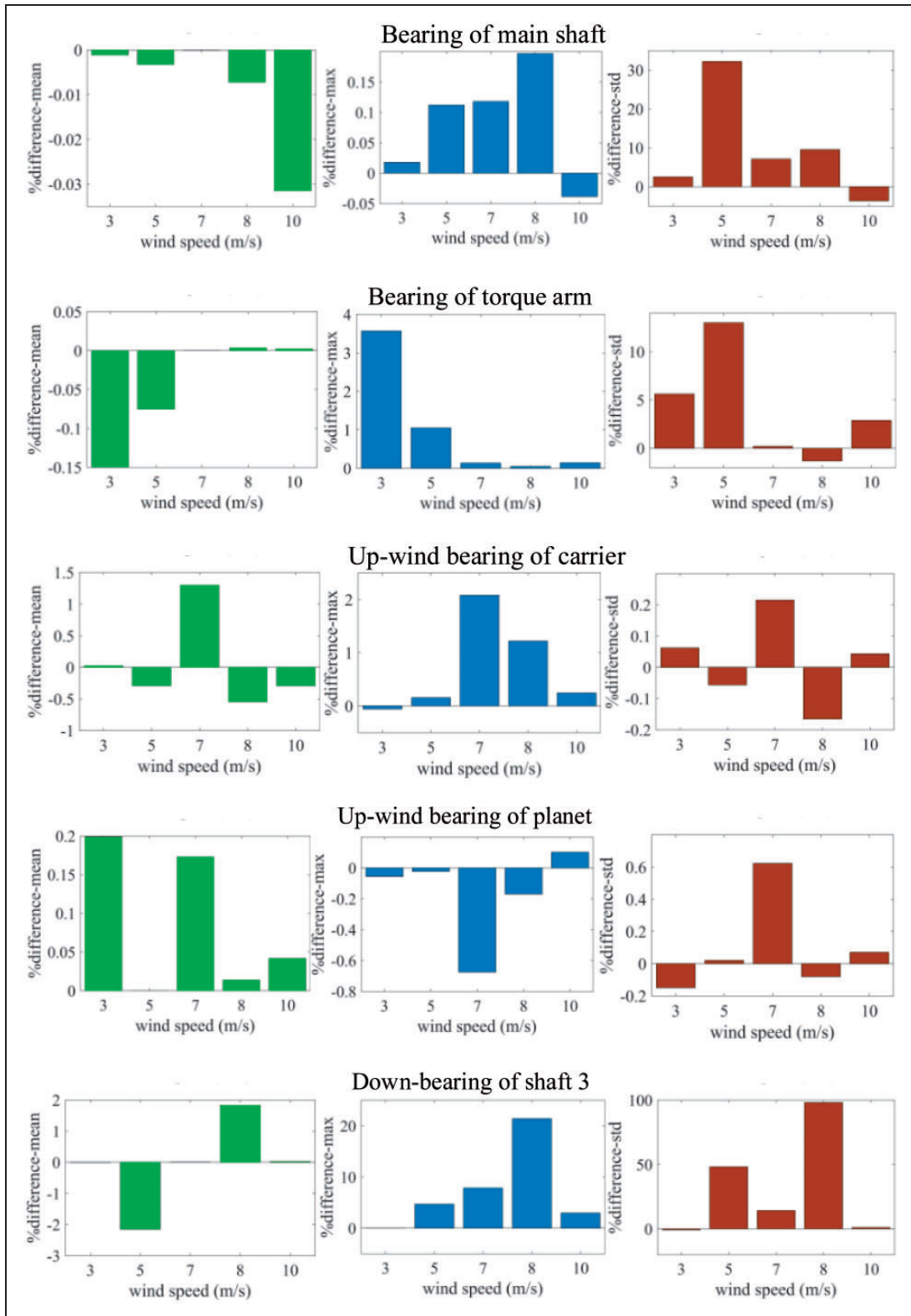


Figure 12. Comparisons of mean values, maximum values and standard deviations along y direction. (a) Bearing of main shaft, (b) bearing of torque arm, (c) upwind bearing of carrier, (d) upwind bearing of planet and (e) downbearing of shaft 3.

acquisition system of SKF Wind, shown in Figure 14(a), and an online monitoring system for vibration measurement of wind turbine drivetrain were built. The vibration performance of the drive train was collected through the acceleration sensors as shown in

Figure 14(b), which was used to measure the vibrations of structure, main shaft bearing, torque arm and generator. The rotation of main shaft normally fluctuates at 13 r/min during the rated working condition. Therefore, the sampling rate of the main shaft was set

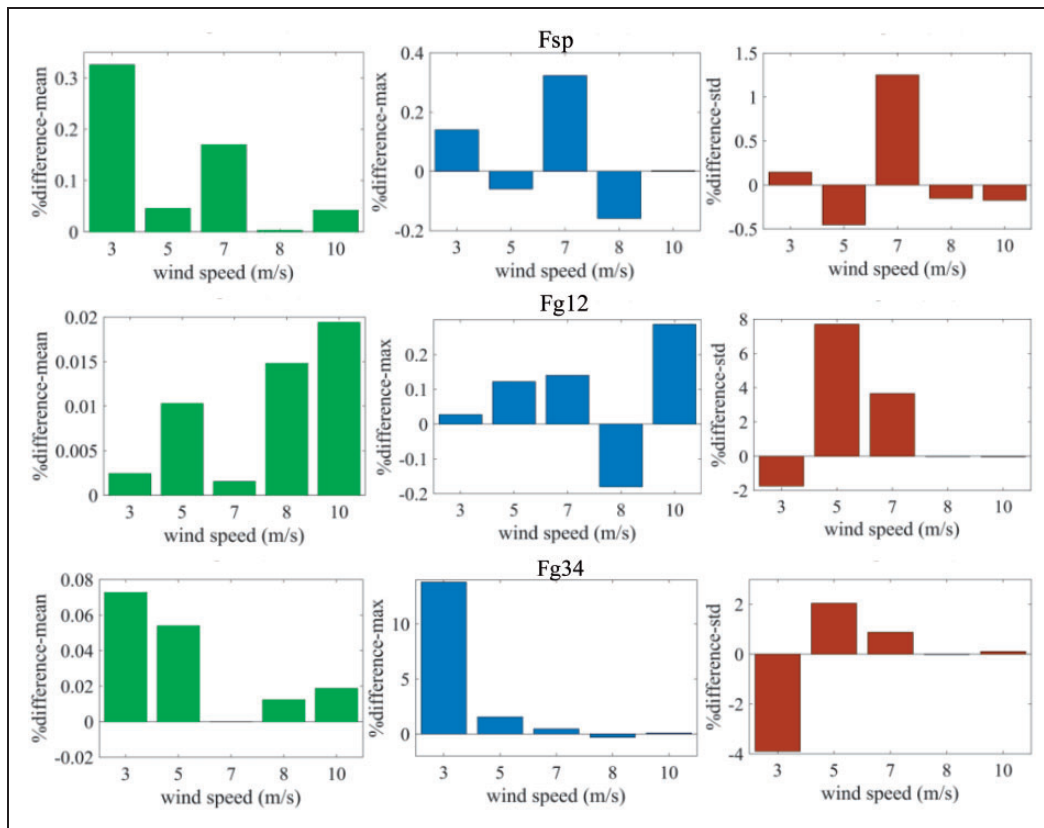


Figure 13. Comparisons of mesh force. (a) Fsp, (b) Fg 12 and (c) Fg 34.

to 2048 Hz, the sampling time was 6.4 s and the frequency resolution was 0.156 Hz. For other measurement points, the sampling rate adopted 10 KHz, the sampling time was 1.28 s and the frequency resolution was 0.78 Hz.

For the test in wind field, the wind speed and generator speed were fluctuated at a wide range, and the wind turbine can change the pitch angle to trace the optimum output power under the rated working condition. In this paper, the wind speed and generator speed as shown in Figure 15 were intercepted as section A, where the generator was working in stable operation stage (about 1782 r/min) and the corresponding wind speed was quite stable (less than 10 m/s). Consequently, the effects of control system on wind turbine drivetrain can be ignored reasonably.

Considering the resolution of measurement sensors as mentioned above, the responses of main shaft and high-speed stage were selected. And the response curves in time domain and frequency domain along y direction and z direction of the main shaft and high-speed stage under the working condition of section A are shown in Figures 16 and 17, respectively. The low-pass filtering in frequency domain was applied to enlarge the frequencies within 5 Hz, which was determined by the rotation frequency and harmonic frequencies of main shaft and swing frequency of tower.

The main frequency is the mesh frequency (139 Hz) and harmonic frequencies of the second stage gear

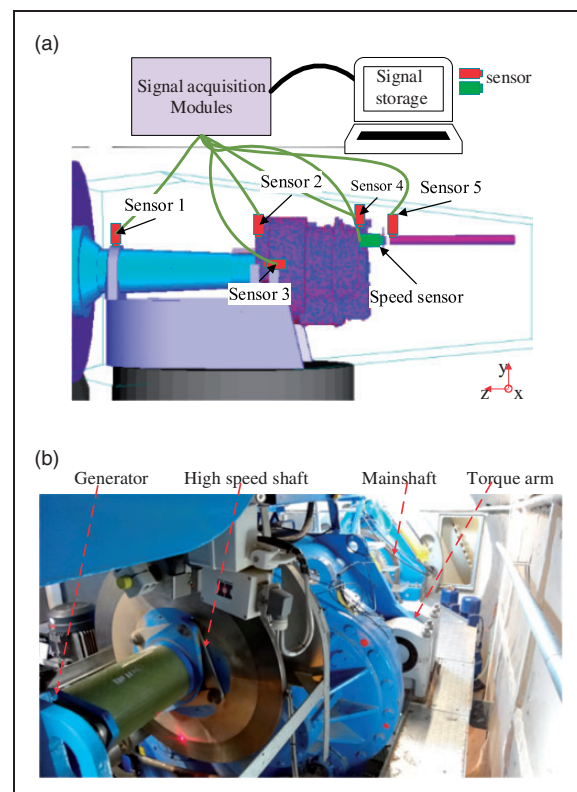


Figure 14. Experiment layout of sensors on the wind turbine drivetrain in wind field. (a) Block-diagram of the experimental system and (b) Locations of the vibration acceleration sensors the experimental system.

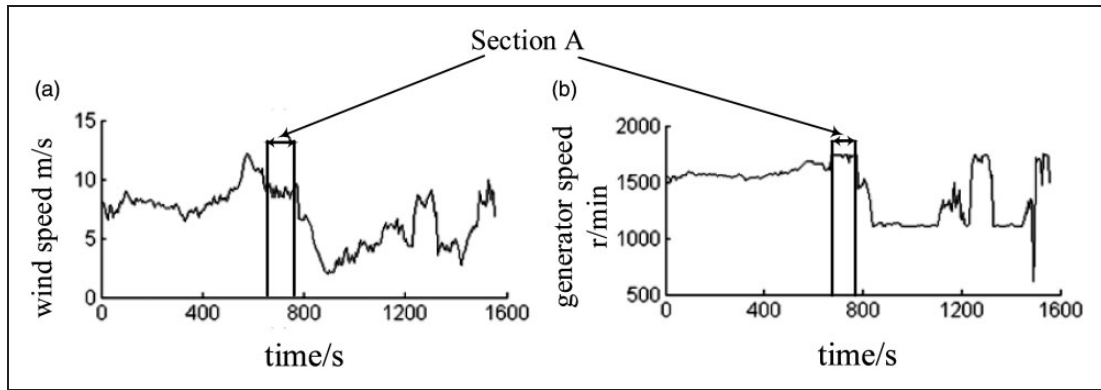


Figure 15. The measured curves of working conditions. (a) the measured wind speed and (b) the speed of generator.

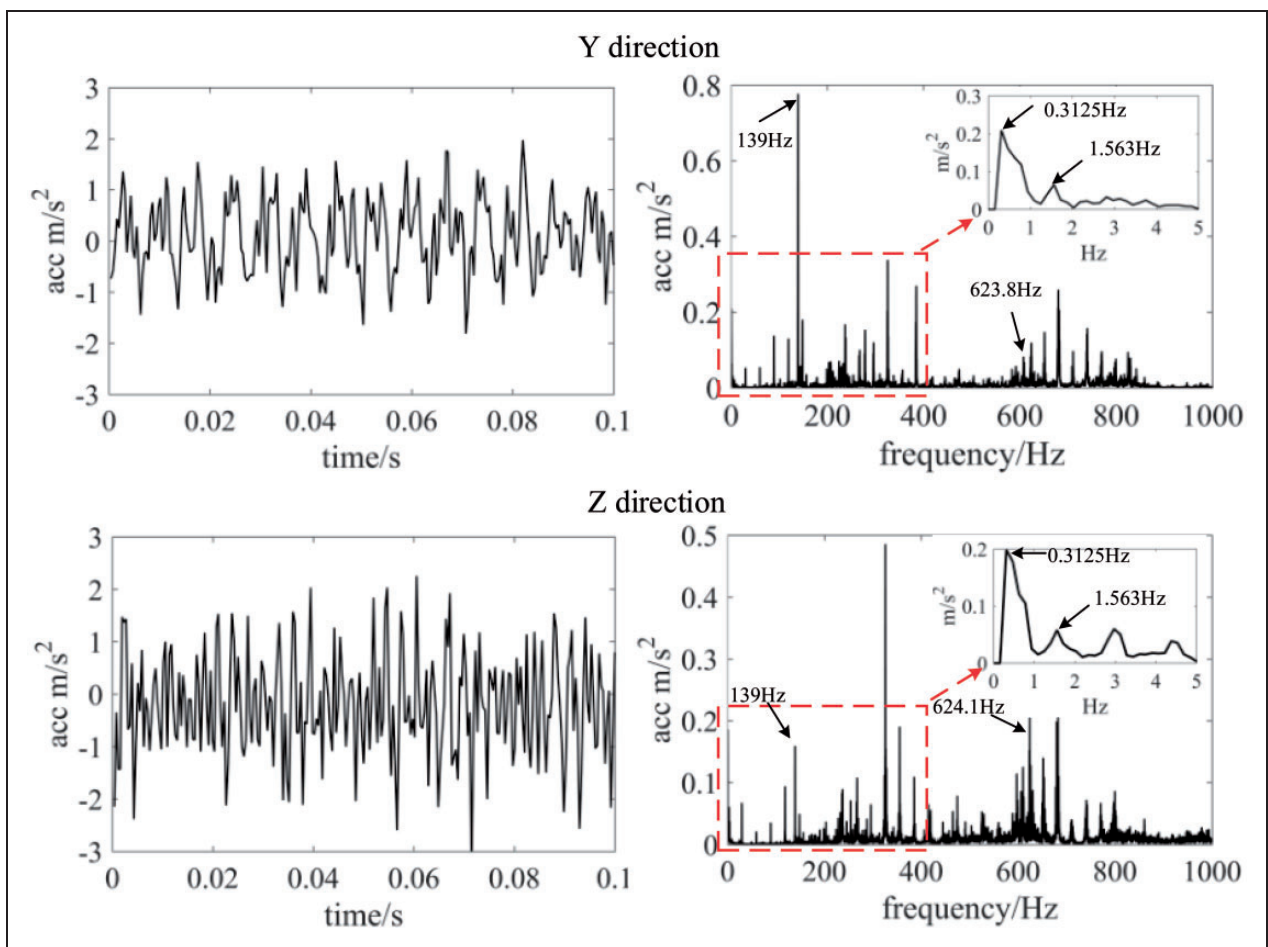


Figure 16. Time-domain curve, spectrogram and low-pass filtering curve of main shaft.

pairs, and the frequencies 624 Hz, 1248 Hz and 1872 Hz are the mesh frequency and harmonic frequencies of the third stage gear pairs, respectively. Therefore, it can be obviously observed that the main dynamic excitations in wind turbine drivetrain are mesh frequencies and harmonic frequencies of gear pairs. As a kind of low-frequency excitation with flexible support of tower, a low-pass filter is adopted to analyze

the effects on the dynamics of wind turbine drivetrain. As seen in Figure 16, it indicates that the vibration acceleration of main shaft exists low-frequency modulation and the main frequencies are 0.3125 Hz and 1.563 Hz. Taking the resolution and the simulation results into account, the results can indicate that 0.3125 Hz and 1.563 Hz are the natural frequencies which are excited by the time-varying wind load.³⁰

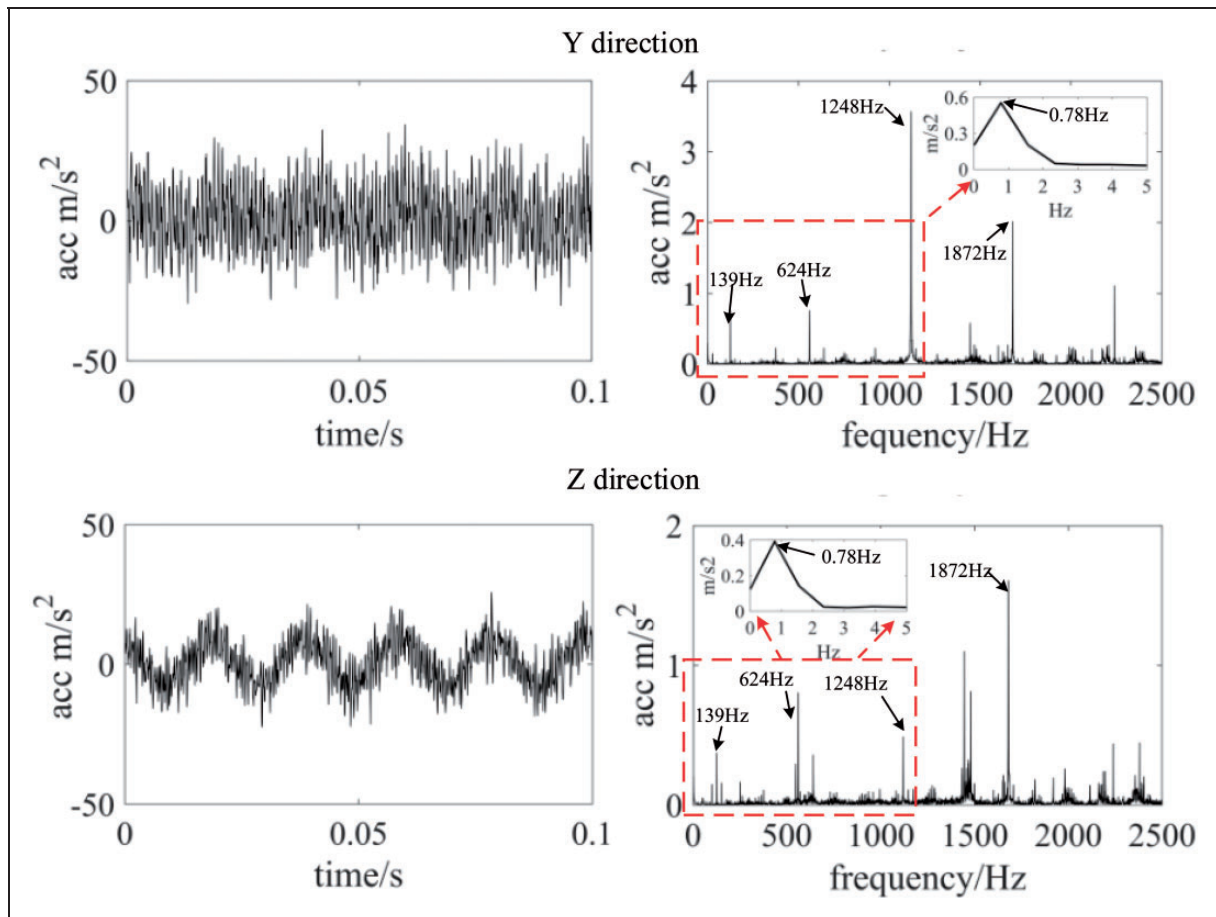


Figure 17. Time-domain curve, spectrogram and low-pass filtering curve of high-speed shaft.

As seen in Figure 17, it can be observed that there is 0.78 Hz at measurement point of high-speed stage, which is caused by frequency resolution (minimum sample rate is 0.78 Hz) of sensors. Hence, the low-frequency excitation of tower swing at carrier, torque arm and high-speed stage needs further investigation. The flexible support can generate a low-frequency excitation at the main shaft as an excitation input to wind turbine drivetrain, which compares well with theoretical analysis.

Conclusion

Based on the dynamic theory for the rigid-flexible coupled system, a dynamic model of wind turbine drivetrain considering flexible supporting was developed according to the basic structure and transmission principle. Using the proposed model, the natural characteristics of the system and dynamic analysis were computed and investigated. The results show that:

(1) The swing mode shapes for the tower in z-direction and x-direction are 0.399 Hz and 0.405 Hz, respectively. And the first natural frequency of drivetrain is 1.64 Hz which represents a torsional vibration mode shape of the drivetrain.

- (2) The potential resonances of the system were investigated by the Campbell diagram and modal energy distribution theory. Although the rotate frequencies of shaft, the mesh frequencies of gear pairs and their harmonic frequencies intersect with the natural frequencies of the system, and resonances would not occur within the normal operating speed range.
- (3) The comparison analysis was conducted to show that the flexible support can increase the axial loads distribution, especially in planetary stage associated with large wind loads, and the radial loads at main shaft and torque arm also can be increased. As a role to isolate the external loads, the flexible support can slightly decrease the mean values of mesh force in planetary stage and decrease the standard deviations of bearing force.
- (4) An experimental remote real-time system was developed to monitor the vibration performance of drive train in the field. And the experimental results correlate well with the simulation.

Declaration of Conflicting Interests

The author(s) declared no potential conflicts of interest with respect to the research, authorship, and/or publication of this article.

Funding

The author(s) disclosed receipt of the following financial support for the research, authorship, and/or publication of this article: The authors appreciate the financial support from the National Natural Science Foundation of China (Grant Nos. 51405043, 51575060) and Chongqing Innovation Program (Nos. cstc2015zdcy-ztxx70010, cstc2015zdcy-ztxx70012).

References

- Helsen J, Vanhollenbeke F, De Coninck F, et al. Insights in wind turbine drive train dynamics gathered by validating advanced models on a newly developed 13.2MW dynamically controlled test-rig. *Mechatronics* 2011; 21: 737–752.
- Peeters J, Vandepitte D, Sas P, et al. Comparison of analysis techniques for the dynamic behaviour of an integrated drivetrain in a wind turbine. In: *International Conference on Noise and Vibration Engineering*, Leuven, Belgium, 16–18 September 2002, Vol. 1–5, pp.1397–1405.
- Lin L, Yang H and Burnett J. Investigation on wind power potential on Hong Kong islands – an analysis of wind power and wind turbine characteristics. *Renewable Energy* 2002; 27: 1–12.
- Quilligan A, O'Connor A and Pakrashi V. Fragility analysis of steel and concrete wind turbine towers. *Eng Struct* 2012; 36: 270–282.
- Muyeen SM, Ali MH, Takahashi R, et al. Comparative study on transient stability analysis of wind turbine generator system using different drive train models. *Iet Renewable Power Gener* 2007; 1: 131–141.
- Stol K and Bir G. Validation of a symbolic wind turbine structural dynamics model. *Cell Biochem Funct* 2000; 22: 206–206.
- Stol K, Balas M and Bir G. Floquet modal analysis of a teetered-rotor wind turbine. *J Solar Energy Eng* 2002; 124: 364–371.
- Todorov M, Dobrev I and Massouh F. Analysis of torsional oscillation of the drive train in horizontal-axis wind turbine. In: *8th International Symposium on Advanced Electromechanical Motion Systems |EPE Chapter Electric Drives Join Symposium*, Lille, France, 1–3 July 2009, pp.56–62.
- Ahlström A. *Aeroelastic simulation of wind turbine dynamics*. Doctoral thesis, Department of Mechanics, Royal Institute of Technology, Sweden, 2005.
- Girsang IP, Dhupia JS, Muljadi E, et al. Gearbox and drivetrain models to study dynamic effects of modern wind turbines. *IEEE Trans Ind Appl* 2014; 50: 3777–3786.
- Peeters JL, Vandepitte D and Sas P. Analysis of internal drive train dynamics in a wind turbine. *Wind Energy* 2006; 9: 141–161.
- Peeters J, Vandepitte D and Sas P. Multibody simulation of a three-stage planetary gearbox in a wind turbine. In: *Proceedings of the 7th German wind Energy conference*, Wilhelmshaven, Germany, 20–21 October 2004.
- Helsen J, Vandepitte D, Desmet W, et al. From torsional resonance analysis towards more degrees of freedom and flexible multibody modelling as a means for improving accuracy of dynamic load prediction in multi-megawatt wind turbine gearboxes. In: *Scientific Proceedings of the European Wind Energy Conference & Exhibition. European Wind Energy Conference*, Marseille, France, 16–19 March 2009, pp.130–136.
- Lee D, Hodges DH and Patel MJ. Multi-flexible-body dynamic analysis of horizontal axis wind turbines. *Wind Energy* 2002; 5: 281–300.
- Hodges D and Patil M. Multi-flexible-body analysis for application to wind-turbine control design. In: *Proceedings of the 19th ASME Wind Energy Symposium*, Reno, Nevada, 10–13 January 2000.
- Oyague F. *Gearbox modeling and load simulation of a baseline 750-kW wind turbine using state-of-the-art simulation codes*. Technical report, National Renewable Energy Laboratory, United States, 2009.
- Sethuraman L, Guo Y and Sheng S. Main bearing dynamics in three-point suspension drivetrains for wind turbines. In: *Awea's WINDPOWER 2015*, Orlando, Florida, 18–21 May 2015.
- Zhu CC, Xu L, Ma F, et al. Remote real-time online testing and evaluation for a megawatt level wind turbine gearbox. *J Vibr Shock* 2012; 31: 17–22.
- Zhu C, Chen S, Song C, et al. Dynamic analysis of a megawatt wind turbine drive train. *J Mech Sci Technol* 2015; 29: 1913–1919.
- Zhu C, Chen S, Liu H, et al. Dynamic analysis of the drive train of a wind turbine based upon the measured load spectrum. *J Mech Sci Technol* 2014; 28: 2033–2040.
- Tamura J, Yamazaki T, Ueno M, et al. Transient stability simulation of power system including wind generator by PSCAD/EMTDC. In: *Power Tech Proceedings of 2001 IEEE Porto*, Porto, Portugal, 10–13 September 2001, pp.1636–1645.
- Abdin ES and Xu W. Control design and dynamic performance analysis of a wind turbine-induction generator unit. *IEEE Trans Energy Conver* 2000; 15: 91–96.
- Schlecht B, Schulze T and Hähnel T. Multibody-system-simulation of wind turbines for determination of additional dynamic loads. In: *SIMPACK Users Meeting*, 9–10 November 2004.
- Kochmann M and Ristow M. Simulation of drivetrains on wind turbines within the framework of certification with Simpack. *SIMPACK News*, 2010, 20–21.
- Xing Y, Karimirad M and Moan T. Modelling and analysis of floating spar-type wind turbine drivetrain. *Wind Energy* 2014; 17: 565–587.
- SIMPACK, Multi-body simulation software, www.simpack.com/related_content.html?cid=2201&pid=707&no_cache=1. (accessed 24 January 2017).
- Hau E and Renouard HV. Windturbines: fundamentals, technologies, application, economics. *Int J Acoust Vibr* 2006; 19: 48.
- Lloyd G. *Guideline for the certification of Wind Turbines*. Hamburg, Germany: Germanischer Lloyd, 2010.
- SKF. WindCon by SKF condition monitoring for wind turbine systems, www.skf.com/files/190928.pdf (accessed 24 January 2017).
- Sheng-lin Z, Cai-chao Z, Sheng SC, et al. Dynamic characteristics analysis of wind turbine drive train with flexible supporting. *J Vibr Shock* 2016; 35: 44–51.